Pseudoparticle approach for charge-transferring molecule-surface collisions

Johannes Marbach,* Franz Xaver Bronold, and Holger Fehske
Institut für Physik, Ernst-Moritz-Arndt-Universität Greifswald, 17489 Greifswald, Germany
(Received 29 June 2012; published 14 September 2012)

Based on a semiempirical generalized Anderson-Newns model, we construct a pseudoparticle description for electron emission due to deexcitation of metastable molecules at surfaces. The pseudoparticle approach allows us to treat resonant charge-transfer and Auger processes on an equal footing, as it is necessary when both channels are open. This is, for instance, the case when a metastable $N_2(^3\Sigma_u^+)$ molecule hits a diamond surface. Using nonequilibrium Green functions and physically motivated approximations to the self-energies of the Dyson equations, we derive a system of rate equations for the probabilities with which the metastable $N_2(^3\Sigma_u^+)$ molecule, the molecular ground state $N_2(^1\Sigma_g^+)$, and the negative ion $N_2^-(^2\Pi_g)$ can be found in the course of the scattering event. From the rate equations, we also obtain the spectrum of the emitted electron and the secondary electron emission coefficient. Our numerical results indicate the resonant tunneling process undermining the source of the Auger channel, which therefore contributes only a few percent to the secondary electron emission.

DOI: 10.1103/PhysRevB.86.115417 PACS number(s): 34.35.+a, 34.70.+e, 79.20.Fv, 79.20.Hx

I. INTRODUCTION

Charge exchange processes during atom-surface or molecule-surface collisions have been the subject of intense scientific research during the last decades.[1,2] This type of surface reactions is of fundamental interest. It represents a quantum impurity problem where a finite many-body system with discrete quantum states couples to an extended system with a continuum of states which essentially acts as a reservoir for electrons. Under appropriate conditions,[3–5] such an arrangement gives for instance rise to the Kondo effect[6] originally found in metals containing magnetic impurities or to Coulomb blockades as it is discussed in nanostructures.[7]

Besides of being a particular realization of a quantum impurity problem, atom/molecule-surface collisions are also of technological interest, especially in the field of bounded low-temperature plasmas, where this type of surface collisions is the main supplier of secondary electrons, which in turn strongly affect the overall charge balance of the discharge.[8] In dielectric barrier discharges, for instance, secondary electron emission determines whether the discharge operates in a filamentary or a diffuse mode.[9,10] Only the latter mode is useful for surface modification. Controlling the yield with which secondary electrons are produced is thus of great practical interest. This applies even more so to microdischarges[11] where the continuing miniaturization gives charge-transferring surface reactions more and more influence on the properties of the discharge.

Depending on the projectile and the target, secondary electron emission usually occurs either in the course of a resonant tunneling process or an Auger transition. In some situations, however, both transitions may be energetically allowed and hence contribute to the yield with which electrons are released. The interplay of the two reaction channels has therefore been studied in the past.[12–21] Starting with the work of Alvarez *et al.*,[17] a detailed theoretical analysis of the interference of Auger and resonant tunneling processes has been given by Goldberg and coworkers.[18,20,21] Their results for H^+ and He^+ indicate the Auger channel to be active only close to the surface whereas the resonant channel is already efficient at rather large projectile-surface distances. When both channels are coupled together, the dynamics of the system is hence controlled by the resonant channel as it destroys the initial species before the Auger channel can become operative. The Auger channel is therefore strongly suppressed in the coupled system albeit the individual efficiencies of the reaction channels are comparable. Onufriev and Marston[14] also investigated the interplay of tunneling and Auger processes for the particular case of Li(2p) atoms deexciting on a metallic surface. Using a sophisticated many-body theoretical description of the scattering process, they concluded that depending on the model parameters, the two deexcitation channels interfere either constructively or destructively.

Whereas the previous studies focused on atomic projectiles, we will investigate in the following the interplay of Auger and resonant tunneling processes for a molecular projectile. More precisely, we will analyze how these two processes affect secondary electron emission due to deexcitation of metastable molecules. Neutralization of molecular ions[22–24] will not be discussed. A particularly interesting case is the deexcitation of metastable $N_2(^3\Sigma_u^+)$ because this molecule deexcites in two primary reaction channels.[25,26] On the one hand, there is the two-step resonant charge transfer (RCT) reaction

$$e_{\vec{k}}^- + N_2(^3\Sigma_u^+) \xrightarrow{\text{RCT}} N_2^-(^2\Pi_g) \xrightarrow{\text{RCT}} N_2(^1\Sigma_g^+) + e_{\vec{q}}^-, \qquad (1)$$

where $e_{\vec{k}}^-$ and $e_{\vec{q}}^-$ denote an electron within the surface and a free electron, respectively. In this process, the metastable $N_2(^3\Sigma_u^+)$ molecule first resonantly captures an electron from the surface to form the intermediate negative ion shape resonance $N_2^-(^2\Pi_g)$ which then decays into the ground state $N_2(^1\Sigma_g^+)$ by resonantly emitting an electron. The decay of the negative ion can be either due to the ion's natural life time or due to the ion surface interaction. In addition to the RCT channel, there exists an Auger deexcitation reaction also known as Penning deexcitation:

$$e_{\vec{k}}^- + N_2(^3\Sigma_u^+) \xrightarrow{\text{Auger}} N_2(^1\Sigma_g^+) + e_{\vec{q}}^-. \qquad (2)$$

Here, the molecule nonresonantly captures a surface electron and simultaneously releases another electron. Depending on the surface band structure, both processes may be possible at

 ©2012 American Physical Society

the same time. This is for instance the case for diamond as it possesses a rather wide valence band.

In our previous work,[27,28] we investigated the two reaction channels separately by a quantum kinetic approach and a rate equation technique. The molecule was in both cases treated as a semiempirical two-level system corresponding to the $2\pi_u$ and $2\pi_g$ molecular orbitals, which are the two molecular orbitals whose occupancies change during the deexcitation process. Spectator electrons not involved in the processes were neglected. Depending on the process, the two levels denoted the upper and lower ionization levels of either the metastable molecule (Auger deexcitation) or the negative ion (resonant charge transfer). The advantage of a semiempirical model is that it is based on a few parameters that are relatively easy accessible, either experimentally or theoretically. The difference of the two parameter sets, which arises from intramolecular Coulomb correlations not included in the model, is not a problem as long as the two processes are treated separately. A simultaneous treatment of them requires, however, a way to implement both parametrizations within a single Hamiltonian.

A way to overcome the problem would be of course to set up a more general projectile Hamiltonian, including active and spectator electrons and their mutual Coulomb interactions. Treating these intramolecular Coulomb correlations explicitly is, however, extremely demanding. It embraces a full quantum chemical description of the approaching molecule that cannot easily be adapted from one projectile to another. Since we are primarily interested in developing models and tools to be used for the description of secondary electron emission from plasma walls, easy adaptation from one projectile-target combination to another is, however, an important criterion for us. We stay therefore within the limits of a semiempirical two-level system and use instead projection operators and two auxiliary bosons to assign and control the level energies. With these constructs, it is possible to formulate a Hamiltonian containing both channels—(1) and (2)—without introducing intramolecular interactions. The projection operators allow us to assign different parametrizations to the two levels, depending on the occupancy of the system, whereas the auxiliary bosons enable us to mimic the intramolecular Coulomb correlations which need to kick in to make the two tunneling processes involved in (1) resonant. Expressing the projection operators in terms of pseudoparticle operators with boson or fermion statistics opens then the door for employing nonequilibrium Green functions to derive from the Hamiltonian quantum kinetic equations for the probabilities with which the molecular states can be found in the course of the collision.

The strength and flexibility of the pseudoparticle or slave field approach, originally developed by Coleman[29] in the context of the infinite-U Anderson Hamiltonian, has been demonstrated many times for Anderson-type and Anderson-Newns-type models.[5,30–33] We apply this method to a generalized Anderson-Newns model describing the coupling of different molecular configurations to a solid. It is of the type but not identical to the model introduced by Marston and coworkers.[14,34] The derivation of the quantum kinetic equations for the pseudoparticle propagators with the subsequent reduction to the rate equations for the occupancies of the molecular pseudoparticle states follows the work of Langreth and coworkers.[5,31] As a result, we obtain rate equations describing the deexcitation of $N_2(^3\Sigma_u^+)$ in situations where the RCT and the Auger channel are simultaneously open. In the absence of the Auger channel, the rate equations reduce to the ones we derived intuitively before for the isolated RCT channel.[28] Applying the model to the particular case of a diamond surface shows the resonant process dominating the Auger process. The overall secondary electron emission coefficient due to deexcitation of $N_2(^3\Sigma_u^+)$ at a diamond surface is on the order of 10^{-1}.

The outline of the rest of the paper is as follows. In Sec. II, we describe the semi-empirical model on which our investigation of the deexcitation process is based. Thereafter, we explain in Sec. III the pseudoparticle representation. Afterwards, we conduct in Sec. IV a second order quantum kinetic calculation on top of the pseudoparticle model. In Sec. V, we introduce a physically motivated semiclassical approximation that allows us to reduce the set of Dyson equations to a set of rate equations. Finally, we present in Sec. VI the results for the diamond surface and conclude in Sec. VII with a brief summary of the main points of the work. Appendix A lists the Langreth-Wilkins rules[35] as used in our calculation and Appendix B collects the second-order Dyson equations for the molecular Green functions.

II. MODEL

The interacting molecule-surface system is characterized by three different types of electronic states: bound and unbound molecular states and states within the solid surface. In the spirit of our previous work,[27,28] we restrict the attention to those states whose occupancies change during the molecule-surface collision. For these states and the coupling between them, we construct a semiempirical model. Its matrix elements can be either obtained from quantum mechanical calculations based on particular assumptions about the electron wave functions and/or experimentally measured ionization energies, electron affinities, surface response functions, and electron tunneling rates. Since we are primarily interested in the quantum kinetic handling of the semiempirical model, we pursue for simplicity the former route. A more realistic parametrization of the model is, however, in principle, possible.

We treat the relevant bound states of the nitrogen molecule in terms of a two-level system consisting of a ground state level "0" and an excited level "1." Within a linear combination of atomic orbital (LCAO) description of the molecule, these two levels represent the nitrogen molecule's $2\pi_u$ and $2\pi_g$ orbitals. Each of the two orbitals can carry four electrons. We neglect, however, the three electrons in the $2\pi_u$ orbital and the three holes in the $2\pi_g$ orbital, which are not directly involved in the deexcitation process. They act only as frozen-in spectators. For the same reason, we neglect the electron spin and treat the magnetic quantum number $m = \pm 1$ as an initial parameter. Hence both levels of our model carry at most one electron.

The two-level system represents any of the molecular states depicted in Fig. 1. The positive ion $N_2^+(^2\Pi_u)$, the ground state $N_2(^1\Sigma_g^+)$, the metastable state $N_2(^3\Sigma_u^+)$, and the negative ion $N_2^-(^2\Pi_g)$. Depending on the particular occupation, the energies ε_0 and ε_1 correspond therefore to the ionization energies of different molecular states. Due to intramolecular

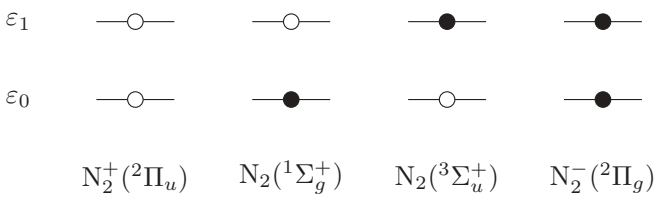

FIG. 1. Correspondence between the occupation of the two-level system and the molecular states. Here, ε_0 and ε_1 denote the energies of the levels 0 and 1, respectively.

Coulomb interactions, these ionization energies are, in general, different.[36,37] We have to allow therefore ε_0 and ε_1 to depend on the occupancy of the two-level system, that is, on the molecular state, it is supposed to represent. In addition, the ionization energies are also subject to the surface's image potential $V_i(z)$ and thus vary with time as the molecule moves with respect to the surface. Using the analysis presented in Ref. 28, we find

$$\varepsilon_{0g}(z) = \varepsilon_{0g}^{\infty} - V_i(z), \tag{3a}$$
$$\varepsilon_{1*}(z) = \varepsilon_{1*}^{\infty} - V_i(z), \tag{3b}$$
$$\varepsilon_{0-}(z) = \varepsilon_{0-}^{\infty} + V_i(z), \tag{3c}$$
$$\varepsilon_{1-}(z) = \varepsilon_{1-}^{\infty} + V_i(z), \tag{3d}$$

where the subscripts g, $*$, and $-$ signal the dependence of the energy levels on the molecular state denoting, respectively, the ground-state molecule, the metastable molecule, and the negative ion. The unperturbed molecular energies are given by[36,37]

$$\begin{aligned} \varepsilon_{0g}^{\infty} &= -17.25\,\text{eV}, \quad \varepsilon_{1*}^{\infty} = -9.67\,\text{eV}, \\ \varepsilon_{0-}^{\infty} &= -14.49\,\text{eV}, \quad \varepsilon_{1-}^{\infty} = 1.18\,\text{eV}. \end{aligned} \tag{4}$$

The overall energy scheme of the coupled molecule-surface system is sketched in Fig. 2 for the particular case of a diamond surface. As can be seen the positive ion is neither involved in the RCT nor the Auger process.

For the image potential, we employ for simplicity the classical expression

$$V_i(z) \approx -\frac{\varepsilon_r^b - 1}{\varepsilon_r^b + 1} \frac{e^2}{16\pi\varepsilon_0} \frac{1}{z}, \tag{5}$$

with ε_r^b standing for the surface's static bulk dielectric constant. Close to the surface, the image potential is, however, truncated according to $V_i(z_c) = V_0$, where V_0 is the depth of the potential barrier confining the electrons of the solid participating in the deexcitation process. As in our previous investigations,[27,28] we describe the solid by a step potential of depth V_0. For a metallic surface,[27] the step depth is the width of the conduction band $\Delta\varepsilon_C$, that is, the sum of the work function Φ_W and the Fermi energy ε_F, whereas for a dielectric surface,[28] it is the sum of the width of the valence band $\Delta\varepsilon_V$, the energy gap ε_g, and the electron affinity ε_α, which can be positive or negative.

In both the RCT and the Auger channel, the emitted electron stems from the molecule and, thus, the emission proceeds into the molecular continuum states. We model the latter as free electron states moving along with the molecule and label them with $\vec{q}$. Electrons residing in those states are also affected by

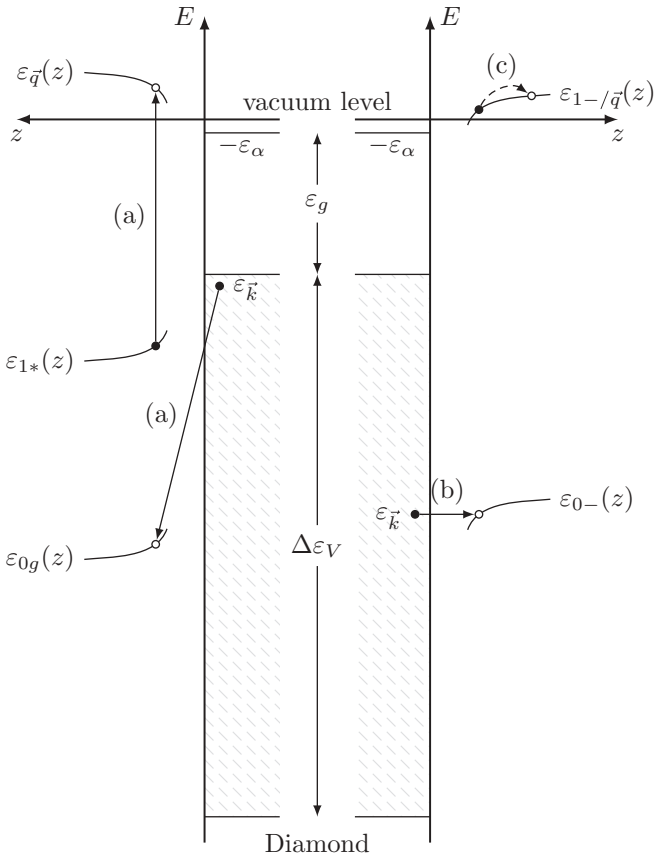

FIG. 2. Energy scheme for the case of a metastable $N_2(^3\Sigma_u^+)$ molecule interaction with a diamond surface. The Auger deexcitation channel (a) is depicted on the left-hand side, whereas the RCT electron capture (b) and the subsequent RCT electron release (c) are shown on the right-hand side. The latter transition is drawn with a dashed line because the electron emission actually occurs at the same z position and hence energy. It is resonant. Therefore the emitted electron will only reach the shown location over time. The drawing is to scale in terms of energy units.

the image potential and their energy is thus given by

$$\varepsilon_{\vec{q}}(z) = \varepsilon_{\vec{q}}^{\infty} + V_i(z) = \frac{\hbar^2 q^2}{2m_e} + V_i(z). \tag{6}$$

The wave function of the emitted electron is a two-center Coulomb wave for the Auger channel[27] and a plane wave for the RCT channel.[28] The latter is a special case of the former that holds for zero effective nucleus charge. Since in the RCT channel the emitted electron leaves a neutral molecule behind, the plane wave is the suitable choice for this channel. In the Auger channel, however, the emitted electron feels the residual two-center Coulomb attraction of the ion core. The two-center Coulomb wave takes this effect into account. To complete the description of the model, we note that we use LCAO molecular wave functions for the two-level system and eigenstates of a step potential for the single-electron wave functions of the solid. Explicit expressions for the wave functions and the details of the calculation of the Auger and tunneling matrix elements are given in Refs. 27 and 28.

Clearly, the model just described is based on a simple surface potential. Modeling the surface potential as a

superposition of a step potential (which somewhat underestimates the exponential tail of the metal electron's wave functions and hence the absolute value of the matrix elements) and a classical image potential (which is less critical because the turning point turns out to be far in front of the surface) allows us, however, to write down analytic expressions for the matrix elements. For the quantum kinetics itself, the matrix elements are only parameters. Our approach can thus be also furnished with improved matrix elements obtained from more realistic potentials. Based on the work of Kürpick and Thumm,[38] we would expect, however, not too dramatic differences.

We now cast the semiempirical model just described into a mathematical form. Introducing projection operators

$$P^{n_0 n_1} = |n_0 n_1\rangle\langle n_0 n_1| \tag{7}$$

projecting onto states of the two-level system with $n_0 = 0,1$ electrons in the lower and $n_1 = 0,1$ electrons in the upper state, the transitions shown in Fig. 2 give rise to a generalized Anderson-Newns model,[34]

$$\begin{aligned} H(t) = &\sum_{\vec{k}} \varepsilon_{\vec{k}}\, c_{\vec{k}}^\dagger c_{\vec{k}} + \sum_{\vec{q}} \varepsilon_{\vec{q}}(t)\, c_{\vec{q}}^\dagger c_{\vec{q}} + \omega_0 b_0^\dagger b_0 + \omega_1 b_1^\dagger b_1 \\ &+ \sum_{n_0,n_1} P^{n_0 n_1}\left[\varepsilon_0^{n_0 n_1}(t)\, c_0^\dagger c_0 + \varepsilon_1^{n_0 n_1}(t)\, c_1^\dagger c_1\right] \\ &+ \sum_{\vec{k}} \left[(P^{01}+P^{11}) V_{\vec{k}}(t)\, c_{\vec{k}}^\dagger b_0^\dagger c_0 + \text{H.c.}\right] \\ &+ \sum_{\vec{q}} \left[(P^{10}+P^{11}) V_{\vec{q}}(t)\, c_{\vec{q}}^\dagger b_1^\dagger c_1 + \text{H.c.}\right] \\ &+ \sum_{\vec{k}\vec{q}} \left[(P^{10}+P^{01}) V_{\vec{k}\vec{q}}(t)\, c_0^\dagger c_{\vec{k}}\, c_{\vec{q}}^\dagger c_1 + \text{H.c.}\right], \end{aligned} \tag{8}$$

where $\varepsilon_0^{10} = \varepsilon_{0g}$, $\varepsilon_1^{01} = \varepsilon_{1*}$, $\varepsilon_0^{11} = \varepsilon_{0-}$, and $\varepsilon_1^{11} = \varepsilon_{1-}$. The remaining energy levels need not be specified further. They drop out in the course of the pseudoparticle representation presented in the next section. The two auxiliary bosons $b_0^{(\dagger)}$ and $b_1^{(\dagger)}$ mimic the intramolecular Coulomb correlations that make the two steps of the RCT channel (1) resonant. This can be accomplished by setting $\omega_0 = \varepsilon_1^{11} - \varepsilon_1^{01}$ and $\omega_1 = \varepsilon_0^{11} - \varepsilon_0^{10}$. The initial energy of the tunneling electron is then resonant, respectively, with the lower and the upper level of the negative ion. The rest of the Hamiltonian is written in the notation we used in our previous work.[27,28]

The time dependence of the Hamiltonian arises from the trajectory of the molecule's center of mass $\vec{R}(t)$. For simplicity, we assume normal incidence described by the trajectory $\vec{R}(t) = (v_0|t| + z_0)\vec{e}_z$, where v_0 is a constant velocity and z_0 is the molecule's turning point, which can be calculated from a Morse type interaction potential.[27] Employing the trajectory, the z dependence of the molecular energies (3) and the energy of the emitted electron (6) transforms into a time dependence. Similarly, the Auger matrix element $V_{\vec{k}\vec{q}}$ and the two resonant tunneling matrix elements $V_{\vec{k}}$ and $V_{\vec{q}}$ acquire also a time dependence.

The quantum kinetic calculation presented below treats the matrix elements of the Hamiltonian as parameters. We are thus not restricted to the specific approximations to the matrix elements derived in our previous work.[27,28] We could as well use matrix elements from *ab initio* calculations or experimental measurements. The natural decay of the negative ion, described by the rate $\Gamma_n = 1/\tau_n$ with τ_n the natural lifetime of the negative ion, is not included in the Hamiltonian (8). It will be inserted at the end into the final set of rate equations for the molecular occupancies.

III. PSEUDOPARTICLE REPRESENTATION

The projection operators (7) permit us to describe the transitions (1) and (2) by a single Hamiltonian. Depending on the process and thus the occupancy of the molecular levels different matrix elements can be assigned to the Hamiltonian. The projectors also guarantee that the $N_2^+(^2\Pi_u)$ state never occurs. In other words, they ensure that the occupancies of the two molecular levels never vanishes simultaneously. For instance, an electron residing in the upper level can only be released when an electron has been captured in the lower level.

A drawback of the projection operators is that they are not suitable for a diagrammatic treatment, which on the other hand is a powerful tool to set up quantum kinetic equations. To remedy this drawback, we now employ a pseudoparticle approach to express the Hamiltonian (8) in terms of slave fields.[5,29–33] The starting point for this procedure is the completeness condition,

$$|00\rangle\langle 00| + |10\rangle\langle 10| + |01\rangle\langle 01| + |11\rangle\langle 11| = 1, \tag{9}$$

which expresses the fact that the molecule can be only in either one of the configurations depicted in Fig. 1. Introducing pseudoparticle operators $c_+^\dagger$, $c_g^\dagger$, $c_*^\dagger$, and $c_-^\dagger$ that create the positive ion, the ground-state molecule, the metastable molecule, and the negative ion from an abstract vacuum state,

$$|00\rangle = c_+^\dagger|\text{vac}\rangle, \quad |10\rangle = c_g^\dagger|\text{vac}\rangle, \tag{10a}$$

$$|01\rangle = c_*^\dagger|\text{vac}\rangle, \quad |11\rangle = c_-^\dagger|\text{vac}\rangle, \tag{10b}$$

the completeness condition (9) becomes

$$c_+^\dagger c_+ + c_g^\dagger c_g + c_*^\dagger c_* + c_-^\dagger c_- = 1. \tag{11}$$

Using Eqs. (9) and (10), the operators $c_{0/1}^{(\dagger)}$ creating and destroying an electron in the two states of the two-level system can then be written as

$$c_0 = c_0 * 1 = |00\rangle\langle 10| - |01\rangle\langle 11| = c_+^\dagger c_g - c_*^\dagger c_-, \tag{12a}$$

$$c_0^\dagger = c_0^\dagger * 1 = |10\rangle\langle 00| - |11\rangle\langle 01| = c_g^\dagger c_+ - c_-^\dagger c_*, \tag{12b}$$

$$c_1 = c_1 * 1 = |00\rangle\langle 01| + |10\rangle\langle 11| = c_+^\dagger c_* + c_g^\dagger c_-, \tag{12c}$$

$$c_1^\dagger = c_1^\dagger * 1 = |01\rangle\langle 00| + |11\rangle\langle 10| = c_*^\dagger c_+ + c_-^\dagger c_g. \tag{12d}$$

In order to satisfy the anticommutation relations of the $c_{0/1}^{(\dagger)}$, one has to define $c_0|11\rangle = -|01\rangle$ and $c_0^\dagger|01\rangle = -|11\rangle$ (see also Ref. 39). The anticommutator relations then reproduce the completeness condition (11) when either the $c_{g/*}$ are bosonic and the $c_{-/+}$ are fermionic or the $c_{g/*}$ are fermionic and the $c_{-/+}$ are bosonic. Without loss of generality, we choose c_g and c_* to be bosonic and declare the labeling conventions:

$$c_g^{(\dagger)} \longrightarrow b_g^{(\dagger)}, \quad c_*^{(\dagger)} \longrightarrow b_*^{(\dagger)}, \tag{13a}$$

$$c_+^{(\dagger)} \longrightarrow f_+^{(\dagger)}, \quad c_-^{(\dagger)} \longrightarrow f_-^{(\dagger)}. \tag{13b}$$

The constraint (11) reduces then to

$$Q = b_g^\dagger b_g + b_*^\dagger b_* + f_-^\dagger f_- + f_+^\dagger f_+ = 1, \tag{14}$$

where we have introduced the usual pseudoparticle number operator Q to encapsulate the constraint.

Formally, the auxiliary fermion and boson operators are pseudoparticle operators creating and annihilating molecular configurations. The constraint ensures that at any time only one of the four possible molecular configurations is present in the system. The occupancy of a molecular pseudoparticle state is thus at most unity. Hence it represents the probability with which the molecular configuration it describes appears in the course of the scattering event.

Inserting the decomposition (12) into the Hamiltonian (8), making the identifications (13), and collecting only terms which are in accordance with (14) is straightforward. The result is

$$\begin{aligned} H(t) = &\sum_{\vec{k}} \varepsilon_{\vec{k}}\, c_{\vec{k}}^\dagger c_{\vec{k}} + \sum_{\vec{q}} \varepsilon_{\vec{q}}(t)\, c_{\vec{q}}^\dagger c_{\vec{q}} + \omega_0 b_0^\dagger b_0 + \omega_1 b_1^\dagger b_1 \\ &+ \varepsilon_g(t)\, b_g^\dagger b_g + \varepsilon_*(t)\, b_*^\dagger b_* + \varepsilon_-(t)\, f_-^\dagger f_- \\ &- \sum_{\vec{k}} [V_{\vec{k}}(t)\, c_{\vec{k}}^\dagger b_0^\dagger b_*^\dagger f_- + \text{H.c.}] \\ &+ \sum_{\vec{q}} [V_{\vec{q}}(t)\, c_{\vec{q}}^\dagger b_1^\dagger b_g^\dagger f_- + \text{H.c.}] \\ &+ \sum_{\vec{k}\vec{q}} [V_{\vec{k}\vec{q}}(t)\, c_{\vec{k}}\, c_{\vec{q}}^\dagger b_g^\dagger b_* + \text{H.c.}], \end{aligned} \tag{15}$$

where we introduced the abbreviations

$$\varepsilon_g = \varepsilon_0^{10}, \quad \varepsilon_* = \varepsilon_1^{01}, \quad \varepsilon_- = \varepsilon_0^{11} + \varepsilon_1^{11}. \tag{16}$$

Notice, no term in the Hamiltonian contains the operator f_+ or its adjoint. This is by construction because the positive ion $N_2^+(^2\Pi_u)$ is not involved in the two transitions the Hamiltonian is supposed to model. The physical meaning of the various terms in the Hamiltonian is particularly transparent. Consider, for instance, the last term describing the Auger deexcitation. A metastable molecule and an electron from the surface disappear while a ground-state molecule and an Auger electron are created.

The operators f_- and $b_{*/g}$ comply to standard commutation and anticommutation relations. It is thus possible to conduct a nonequilibrium diagrammatic expansion of the interaction terms in Eq. (15). The Hamiltonian (15) conserves the pseudoparticle number Q. The quantum kinetic equations, however, may contain terms that violate the constraint. The projection onto the physical subspace with $Q = 1$ needs to be therefore carried out explicitly. For this purpose, we employ in the next section the Langreth-Nordlander projection technique.[31]

IV. QUANTUM KINETICS

To start the quantum kinetic calculation, we first define a contour-ordered fermion Green function G_- for the negative ion and contour-ordered boson Green functions $B_{*/g/0/1}$ for the metastable molecule, the molecular ground state, and the two auxiliary bosons, respectively. Using the notation of Langreth and Nordlander,[31] we write

$$i G_-(t,t') = \langle T_{\mathcal{C}}\, f_-(t)\, f_-^\dagger(t')\rangle, \tag{17a}$$

$$i B_l(t,t') = \langle T_{\mathcal{C}}\, b_l(t)\, b_l^\dagger(t')\rangle, \tag{17b}$$

where $l = *,g,0,1$, and define the analytic pieces $G_-^{>}$ and $B_l^{>}$ by

$$i G_-(t,t') = \Theta_{\mathcal{C}}(t-t')\, G_-^{>}(t,t') - \Theta_{\mathcal{C}}(t'-t)\, G_-^{<}(t,t'), \tag{18a}$$

$$i B_l(t,t') = \Theta_{\mathcal{C}}(t-t')\, B_l^{>}(t,t') + \Theta_{\mathcal{C}}(t'-t)\, B_l^{<}(t,t'). \tag{18b}$$

The time-ordering operator $T_{\mathcal{C}}$ and the $\Theta_{\mathcal{C}}$ function are defined on a complex time contour. The associated retarded Green functions G_-^R and B_l^R are given by

$$i G_-^R(t,t') = \Theta(t-t')[G_-^{>}(t,t') + G_-^{<}(t,t')], \tag{19a}$$

$$i B_l^R(t,t') = \Theta(t-t')[B_l^{>}(t,t') - B_l^{<}(t,t')], \tag{19b}$$

whereas the advanced functions G_-^A and B_l^A may be constructed from Eq. (19) using the relations

$$G_-^A(t,t') = [G_-^R(t',t)]^*, \tag{20a}$$

$$B_l^A(t,t') = \left[B_l^R(t',t)\right]^*. \tag{20b}$$

In contrast to our previous work,[27,28] we no longer use Keldysh's matrix notation. Langreth's notation is more convenient. It enables us to use the powerful Langreth-Wilkins rules[35] that lead more directly to the quantum kinetic equations for the molecular occupancies, that is, the probabilities with which the molecular configurations involved in the deexcitation process appear in the course of the scattering event.

In order to calculate the self-energies, we truncate the diagrammatic expansion beyond the second order and employ the self-consistent noncrossing approximation.[31] The diagrams for the fermionic self-energy Σ_- and the bosonic self-energies Π_* and Π_g are shown in Fig. 3. Mathematically, they read

$$\Sigma_-(t_1,t_2) = i\, \sigma_{\vec{k}}(t_1,t_2)\, B_*(t_1,t_2) + i\, \sigma_{\vec{q}}(t_1,t_2)\, B_g(t_1,t_2), \tag{21a}$$

$$\Pi_*(t_1,t_2) = -i\, \sigma_{\vec{k}}(t_2,t_1)\, G_-(t_1,t_2) + \sigma_{\vec{k}\vec{q}}(t_1,t_2)\, B_g(t_1,t_2), \tag{21b}$$

$$\Pi_g(t_1,t_2) = -i\, \sigma_{\vec{q}}(t_2,t_1)\, G_-(t_1,t_2) + \sigma_{\vec{k}\vec{q}}(t_2,t_1)\, B_*(t_1,t_2) \tag{21c}$$

with

$$\sigma_{\vec{k}/\vec{q}}(t_1,t_2) = \frac{i}{\hbar^2} \sum_{\vec{k}/\vec{q}} V_{\vec{k}/\vec{q}}^*(t_1)\, V_{\vec{k}/\vec{q}}(t_2) G_{\vec{k}/\vec{q}}^{(0)}(t_1,t_2) B_{0/1}^{(0)}(t_1,t_2), \tag{22a}$$

$$\sigma_{\vec{k}\vec{q}}(t_1,t_2) = -\frac{1}{\hbar^2} \sum_{\vec{k}\vec{q}} V_{\vec{k}\vec{q}}^*(t_1)\, V_{\vec{k}\vec{q}}(t_2) G_{\vec{k}}^{(0)}(t_2,t_1)\, G_{\vec{q}}^{(0)}(t_1,t_2), \tag{22b}$$

and $G_{\vec{q}/\vec{k}}^{(0)}$ and $B_{0/1}^{(0)}$ denoting, respectively, the contour-ordered Green functions for a free/valence band electron and an auxiliary boson.

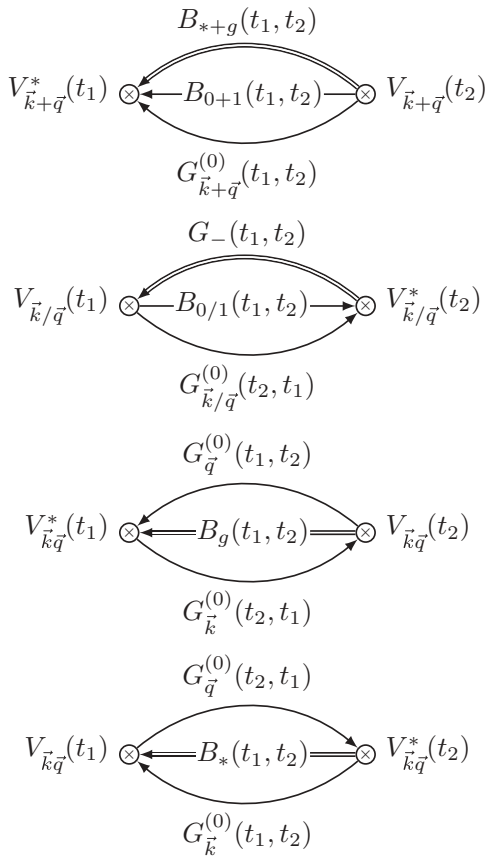

FIG. 3. Second-order self-energy diagrams in self-consistent noncrossing approximation. Depicted are from top to bottom the self-energy of the fermionic level $-i\,\Sigma_-(t_1,t_2)$, the RCT component of the self-energies of the bosonic levels $-i\,\Pi_*(t_1,t_2)$ and $-i\,\Pi_g(t_1,t_2)$, the Auger component of the metastable boson self-energy $-i\,\Pi_*(t_1,t_2)$, and the Auger component of the ground-state boson self-energy $-i\,\Pi_g(t_1,t_2)$. In the upper most diagram, the $+$ sign in the indices means that there are two separate diagrams, one with the $\vec{k}$ and $*$ indices and one with the $\vec{q}$ and g indices, both of which contribute in an additive way and have thus to be summed. Furthermore, in the diagram below, the upper most one the subscripts $\vec{k}$ and 0 hold for Π_* and the subscripts $\vec{q}$ and 1 hold for Π_g. In all diagrams, a double line indicates a full propagator, whereas a single line denotes an unperturbed propagator.

In the self-energies (21), the two reaction channels (1) and (2) are separated. Every term involving $\sigma_{\vec{k}}$ or $\sigma_{\vec{q}}$ refers to the RCT channel and every term containing $\sigma_{\vec{k}\vec{q}}$ pertains to the Auger channel. Due to the dressed Green functions, the two channels are, however, coupled. The Green functions of the auxiliary bosons contained in $\sigma_{\vec{k}}$ and $\sigma_{\vec{q}}$ ensure that the two tunneling processes contained in Eq. (1) are resonant. Physically, the auxiliary bosons simulate the action of intramolecular correlations that kick in when an electron hops to-and-from the molecule.

Using the Langreth-Wilkins rules for analytic continuation (see Refs. 31 and 35 and Appendix A), we obtain from the self-energies (21) the set of Dyson equations given in Appendix A. The components of these equations arising from the RCT terms are equivalent to the ones in Ref. 31 but with two bosonic pseudoparticles instead of one and an energy shift caused by the auxiliary bosons. The set of Dyson equations (B1) contains terms that violate the constraint (14). Before physically meaningful information can be extracted, the Dyson equations have to be projected onto the physical subspace defined by the constraint (14).

The procedure to achieve this is originally due to Langreth and Nordlander and has been outlined several times.[30–32] It is based on inspecting the order of the Green functions in the conserved pseudoparticle number Q. The retarded functions G^R_- and $B^R_{*/g}$ are proportional to Q^0, while the lesser Green functions $G^<_-$ and $B^<_{*/g}$ are proportional to Q^1. Thus we have to omit any terms of higher order than Q^0 from the retarded self-energies and any terms of higher order than Q^1 from the lesser self-energies. This approach is not an additional approximation but an exact projection enforced by the constraint.[31]

Before carrying out the projection, we split off the Green functions' oscillating factors by means of the decompositions[5]

$$G^{</R/A}_-(t,t') = \widetilde{G}^{</R/A}_-(t,t')\,e^{-\frac{i}{\hbar}\int_{t'}^{t} dt_1\,\varepsilon_-(t_1)}, \tag{23a}$$
$$B^{</R/A}_*(t,t') = \widetilde{B}^{</R/A}_*(t,t')\,e^{-\frac{i}{\hbar}\int_{t'}^{t} dt_1\,\varepsilon_*(t_1)}, \tag{23b}$$
$$B^{</R/A}_g(t,t') = \widetilde{B}^{</R/A}_g(t,t')\,e^{-\frac{i}{\hbar}\int_{t'}^{t} dt_1\,\varepsilon_g(t_1)}, \tag{23c}$$

and

$$\widetilde{G}^R_-(t,t') = -i\,\Theta(t-t')\,g_-(t,t'), \tag{24a}$$
$$\widetilde{G}^A_-(t,t') = i\,\Theta(t'-t)\,g_-(t,t'), \tag{24b}$$
$$\widetilde{B}^R_{*/g}(t,t') = -i\,\Theta(t-t')\,b_{*/g}(t,t'), \tag{24c}$$
$$\widetilde{B}^A_{*/g}(t,t') = i\,\Theta(t'-t)\,b_{*/g}(t,t'). \tag{24d}$$

Using the definition of the retarded and advanced Green functions, we find the following relations:[5]

$$g_-(t,t) = b_{*/g}(t,t) = 1, \tag{25a}$$
$$g_-(t,t') = [g_-(t',t)]^*, \tag{25b}$$
$$b_{*/g}(t,t') = [b_{*/g}(t',t)]^*. \tag{25c}$$

Within the Dyson equations, the oscillating terms emerging from Eq. (23) will be absorbed in the functions $\widetilde{\sigma}^<_{\vec{k}}$, $\widetilde{\sigma}^>_{\vec{q}}$, and $\widetilde{\sigma}^>_{\vec{k}\vec{q}}$, which are defined by

$$\sigma^<_{\vec{k}}(t,t') = \widetilde{\sigma}^<_{\vec{k}}(t,t')\,e^{-\frac{i}{\hbar}\int_{t'}^{t} dt_1\,[\varepsilon_-(t_1)-\varepsilon_*(t_1)]}, \tag{26a}$$
$$\sigma^>_{\vec{q}}(t,t') = \widetilde{\sigma}^>_{\vec{q}}(t,t')\,e^{-\frac{i}{\hbar}\int_{t'}^{t} dt_1\,[\varepsilon_-(t_1)-\varepsilon_g(t_1)]}, \tag{26b}$$
$$\sigma^>_{\vec{k}\vec{q}}(t,t') = \widetilde{\sigma}^>_{\vec{k}\vec{q}}(t,t')\,e^{-\frac{i}{\hbar}\int_{t'}^{t} dt_1\,[\varepsilon_*(t_1)-\varepsilon_g(t_1)]}. \tag{26c}$$

The terms $\sigma^>_{\vec{k}}$, $\sigma^<_{\vec{q}}$, and $\sigma^<_{\vec{k}\vec{q}}$ vanish identically due to the initial conditions $n_0(t_0) = n_{\vec{k}}(t_0) = 1$ and $n_1(t_0) = n_{\vec{q}}(t_0) = 0$ since

$$\sigma^>_{\vec{k}}(t,t') \sim [1-n_{\vec{k}}(t_0)][1-n_0(t_0)] = 0, \tag{27a}$$
$$\sigma^<_{\vec{q}}(t,t') \sim n_{\vec{q}}(t_0)n_1(t_0) = 0, \tag{27b}$$
$$\sigma^<_{\vec{k}\vec{q}}(t,t') \sim n_{\vec{q}}(t_0) = 0. \tag{27c}$$

Employing the Langreth-Nordlander projection together with the relations (23), (24), (26), and (27), the set of Dyson

equations (B1) takes the following form:

$$\frac{\partial}{\partial t}\widetilde{G}^{<}_{-}(t,t') = -\int_{-\infty}^{t} dt_1\ \widetilde{\sigma}^{>}_{\vec{q}}(t,t_1)\, b_g(t,t_1)\, \widetilde{G}^{<}_{-}(t_1,t') + \int_{-\infty}^{t'} dt_1\ \widetilde{\sigma}^{<}_{\vec{k}}(t,t_1)\, \widetilde{B}^{<}_{*}(t,t_1)\, g_{-}(t_1,t')\ , \tag{28a}$$

$$\frac{\partial}{\partial t}\widetilde{B}^{<}_{*}(t,t') = -\int_{-\infty}^{t} dt_1\ [\widetilde{\sigma}^{<}_{\vec{k}}(t_1,t)\, g_{-}(t,t_1)\, \widetilde{B}^{<}_{*}(t_1,t') + i\widetilde{\sigma}^{>}_{\vec{k}\vec{q}}(t,t_1)\, b_g(t,t_1)\, \widetilde{B}^{<}_{*}(t_1,t')], \tag{28b}$$

$$\frac{\partial}{\partial t}\widetilde{B}^{<}_{g}(t,t') = \int_{-\infty}^{t'} dt_1\ [\widetilde{\sigma}^{>}_{\vec{q}}(t_1,t)\, \widetilde{G}^{<}_{-}(t,t_1)\, b_g(t_1,t') + i\widetilde{\sigma}^{>}_{\vec{k}\vec{q}}(t_1,t)\, \widetilde{B}^{<}_{*}(t,t_1)\, b_g(t_1,t')], \tag{28c}$$

$$\Theta(t-t')\frac{\partial}{\partial t} g_{-}(t,t') = -\int_{t'}^{t} dt_1\ \widetilde{\sigma}^{>}_{\vec{q}}(t,t_1)\, b_g(t,t_1)\, g_{-}(t_1,t'), \tag{28d}$$

$$\Theta(t-t')\frac{\partial}{\partial t} b_{*}(t,t') = -\int_{t'}^{t} dt_1\ [\widetilde{\sigma}^{<}_{\vec{k}/\vec{q}}(t_1,t)\, g_{-}(t,t_1)\, b_{*/g}(t_1,t') + i\widetilde{\sigma}^{>}_{\vec{k}\vec{q}}(t,t_1)\, b_g(t,t_1)\, b_{*}(t_1,t')]\ , \tag{28e}$$

$$\Theta(t-t')\frac{\partial}{\partial t} b_g(t,t') = 0. \tag{28f}$$

The time evolution of the molecular occupation numbers n_-, n_*, and n_g can be calculated from the following relations:[31]

$$\frac{dn_{-}(t)}{dt} = \left.\frac{\partial \widetilde{G}^{<}_{-}(t,t')}{\partial t}\right|_{t=t'} + \left.\frac{\partial \widetilde{G}^{<}_{-}(t,t')}{\partial t'}\right|_{t=t'}, \tag{29a}$$

$$\frac{dn_{*}(t)}{dt} = \left.\frac{\partial \widetilde{B}^{<}_{*}(t,t')}{\partial t}\right|_{t=t'} + \left.\frac{\partial \widetilde{B}^{<}_{*}(t,t')}{\partial t'}\right|_{t=t'}, \tag{29b}$$

$$\frac{dn_{g}(t)}{dt} = \left.\frac{\partial \widetilde{B}^{<}_{g}(t,t')}{\partial t}\right|_{t=t'} + \left.\frac{\partial \widetilde{B}^{<}_{g}(t,t')}{\partial t'}\right|_{t=t'}. \tag{29c}$$

Hence, we also need the adjoint Dyson equations of the lesser functions that can be calculated in the same manner. The result reads

$$\frac{\partial}{\partial t'}\widetilde{G}^{<}_{-}(t,t') = -\int_{-\infty}^{t'} dt_1\ \widetilde{G}^{<}_{-}(t,t_1)\widetilde{\sigma}^{>}_{\vec{q}}(t_1,t')\, b_g(t_1,t') + \int_{-\infty}^{t} dt_1\ g_{-}(t,t_1)\widetilde{\sigma}^{<}_{\vec{k}}(t_1,t')\, \widetilde{B}^{<}_{*}(t_1,t'), \tag{30a}$$

$$\frac{\partial}{\partial t'}\widetilde{B}^{<}_{*}(t,t') = -\int_{-\infty}^{t'} dt_1\ \widetilde{B}^{<}_{*}(t,t_1)\widetilde{\sigma}^{<}_{\vec{k}}(t',t_1)\, g_{-}(t_1,t') - \int_{-\infty}^{t'} dt_1\ \widetilde{B}^{<}_{*}(t,t_1)\, i\widetilde{\sigma}^{>}_{\vec{k}\vec{q}}(t_1,t')\, b_g(t_1,t'), \tag{30b}$$

$$\frac{\partial}{\partial t'}\widetilde{B}^{<}_{g}(t,t') = \int_{-\infty}^{t} dt_1\ b_g(t,t_1)\widetilde{\sigma}^{>}_{\vec{q}}(t',t_1)\, \widetilde{G}^{<}_{-}(t_1,t') + \int_{-\infty}^{t} dt_1 b_g(t,t_1)\, i\widetilde{\sigma}^{>}_{\vec{k}\vec{q}}(t',t_1)\, \widetilde{B}^{<}_{*}(t_1,t'). \tag{30c}$$

Equations (28) and (30) constitute the final projected set of Dyson equations that determines the dynamics of the system within the subspace $Q = 1$. The rate-equation-like structure of these equations is already evident. The Dyson equation for the lesser Green function of the negative ion, Eq. (30a), for instance, contains a production term proportional to $\widetilde{\sigma}^{<}_{\vec{k}}$ and $\widetilde{B}^{<}_{*}$ and a loss term proportional to $\widetilde{\sigma}^{>}_{\vec{q}}$ and $\widetilde{G}^{<}_{-}$. These terms relate to the production and loss of negative ions by the RCT electron capture and release reaction, respectively.

Since the self-energies are known in terms of the Green functions, Eqs. (28) and (30) constitute a closed set of equations. A numerical solution along the lines pioneered by Shao *et al.*[5] could thus be attempted. The rather involved numerics of double-time Green functions is however not required for moderate projectile velocities.[5] In that case, the semiclassical approximation described in the next section can be employed to reduce Eqs. (28) and (30) to a set of rate equations. As far as possible applications of our approach to plasma walls are concerned, we have to keep in mind, however, that plasma walls are usually negatively charged with respect to the bulk plasma. Charged projectiles might thus acquire kinetic energies for which the semiclassical approximation and with it the rate equations are no longer valid. The metastable molecules, however, we are concerned with in the present work approach the surface with thermal energies making the rate equations an excellent approximation to the full two-time equations.

V. SEMICLASSICAL APPROXIMATION

The strongly oscillating factors of the projected set of Dyson equations are contained in the functions $\widetilde{\sigma}^{<}_{\vec{k}}$, $\widetilde{\sigma}^{>}_{\vec{q}}$, and $\widetilde{\sigma}^{>}_{\vec{k}\vec{q}}$. If these functions are strongly peaked along the time diagonal $t = t'$, we can apply a saddle point approximation to the integrals in Eqs. (28) and (30). For instance,

$$\int_{-\infty}^{t'} dt_1\ \widetilde{\sigma}^{<}_{\vec{k}}(t,t_1)\, \widetilde{B}^{<}_{*}(t,t_1)\, g_{-}(t_1,t') \approx \widetilde{B}^{<}_{*}(t,t)\, g_{-}(t,t') \int_{-\infty}^{t'} dt_1\ \widetilde{\sigma}^{<}_{\vec{k}}(t,t_1). \tag{31}$$

The validity of this approximation, which is also known as the semiclassical approximation,[31] will be demonstrated in Sec. VI.

Within the saddle-approximation, the projected Dyson equations for the lesser Green functions become

$$\frac{\partial}{\partial t}\widetilde{G}^{<}_{-}(t,t') \approx -\underbrace{b_g(t,t)}_{1}\widetilde{G}^{<}_{-}(t,t')\int_{-\infty}^{t} dt_1\,\widetilde{\sigma}^{>}_{\vec{q}}(t,t_1) + \widetilde{B}^{<}_{*}(t,t)\,g_{-}(t,t')\int_{-\infty}^{t'} dt_1\,\widetilde{\sigma}^{<}_{\vec{k}}(t,t_1), \tag{32a}$$

$$\frac{\partial}{\partial t'}\widetilde{G}^{<}_{-}(t,t') \approx -\widetilde{G}^{<}_{-}(t,t')\underbrace{b_g(t',t')}_{1}\int_{-\infty}^{t'} dt_1\,\widetilde{\sigma}^{>}_{\vec{q}}(t_1,t') + g_{-}(t,t')\,\widetilde{B}^{<}_{*}(t',t')\int_{-\infty}^{t} dt_1\,\widetilde{\sigma}^{<}_{\vec{k}}(t_1,t'), \tag{32b}$$

$$\frac{\partial}{\partial t}\widetilde{B}^{<}_{*}(t,t') \approx -\underbrace{g_{-}(t,t)}_{1}\widetilde{B}^{<}_{*}(t,t')\int_{-\infty}^{t} dt_1\,\widetilde{\sigma}^{<}_{\vec{k}}(t_1,t) - \underbrace{b_g(t,t)}_{1}\widetilde{B}^{<}_{*}(t,t')\int_{-\infty}^{t} dt_1\,i\widetilde{\sigma}^{>}_{\vec{k}\vec{q}}(t,t_1), \tag{32c}$$

$$\frac{\partial}{\partial t'}\widetilde{B}^{<}_{*}(t,t') \approx -\widetilde{B}^{<}_{*}(t,t')\underbrace{g_{-}(t',t')}_{1}\int_{-\infty}^{t'} dt_1\,\widetilde{\sigma}^{<}_{\vec{k}}(t',t_1) - \widetilde{B}^{<}_{*}(t,t')\underbrace{b_g(t',t')}_{1}\int_{-\infty}^{t'} dt_1\,i\widetilde{\sigma}^{>}_{\vec{k}\vec{q}}(t_1,t'), \tag{32d}$$

$$\frac{\partial}{\partial t}\widetilde{B}^{<}_{g}(t,t') \approx \widetilde{G}^{<}_{-}(t,t)\,b_g(t,t')\int_{-\infty}^{t'} dt_1\,\widetilde{\sigma}^{>}_{\vec{q}}(t_1,t) + \widetilde{B}^{<}_{*}(t,t)\,b_g(t,t')\int_{-\infty}^{t'} dt_1\,i\widetilde{\sigma}^{>}_{\vec{k}\vec{q}}(t_1,t), \tag{32e}$$

$$\frac{\partial}{\partial t'}\widetilde{B}^{<}_{g}(t,t') \approx b_g(t,t')\,\widetilde{G}^{<}_{-}(t',t')\int_{-\infty}^{t} dt_1\,\widetilde{\sigma}^{>}_{\vec{q}}(t',t_1) + b_g(t,t')\,\widetilde{B}^{<}_{*}(t',t')\int_{-\infty}^{t} dt_1\,i\widetilde{\sigma}^{>}_{\vec{k}\vec{q}}(t',t_1). \tag{32f}$$

Using Eqs. (29), we then arrive at a set of rate equations for the occupancies of the molecular pseudoparticle states:

$$\frac{dn_{-}(t)}{dt} \approx -\Gamma_1(t)\,n_{-}(t) + \Gamma_0(t)\,n_{*}(t), \tag{33a}$$

$$\frac{dn_{*}(t)}{dt} \approx -\Gamma_0(t)\,n_{*}(t) - \Gamma_A(t)\,n_{*}(t), \tag{33b}$$

$$\frac{dn_{g}(t)}{dt} \approx \Gamma_1(t)\,n_{-}(t) + \Gamma_A(t)\,n_{*}(t), \tag{33c}$$

where the rates are given by

$$\Gamma_0(t) = \int_{-\infty}^{t} dt_1\; 2\Re[\widetilde{\sigma}^{<}_{\vec{k}}(t,t_1)], \tag{34a}$$

$$\Gamma_1(t) = \int_{-\infty}^{t} dt_1\; 2\Re[\widetilde{\sigma}^{>}_{\vec{q}}(t,t_1)] + \Gamma_n, \tag{34b}$$

$$\Gamma_A(t) = \int_{-\infty}^{t} dt_1\; 2\Re[i\widetilde{\sigma}^{>}_{\vec{k}\vec{q}}(t,t_1)]. \tag{34c}$$

Note, in Eq. (34b), we incorporated the natural decay of the negative ion by adding the natural decay rate $\Gamma_n = 1/\tau_n$ on the right-hand side.

Similar to what Langreth and coworkers did in the context of the neutralization of atomic ions,[5,31] we have thus reduced a complicated set of Dyson equations—Eqs. (28) and (30) describing the deexcitation of a metastable molecule via the simultaneous action of the RCT (1) and the Auger (2) channels—to an easy to handle system of rate equations (33). The reaction rates (34) entering the rate equations are linked to quantum kinetic quantities and thus related to the semiempirical model.

The rates Γ_0 and Γ_1 defined in Eqs. (34a) and (34b) are equal to the rates employed in Ref. 28. Mathematical expressions for these two rates—as obtained from the semiempirical model—can thus be looked up in our previous work.[28] The Auger rate Γ_A introduced in Eq. (34c) however has not been calculated before. Within the semiempirical model, it is given by

$$\Gamma_A(t) = \int_0^{\infty} dq_r\; 2\Re\Bigg\{\frac{[\Gamma_{\vec{k}\vec{q}}(t)]^*}{\hbar^2(\Delta q)^3(\Delta k)^3}\int_{t_0}^{t} dt_1 \times \int_0^{\frac{\pi}{2}} dq_\vartheta \int_0^{2\pi} dq_\varphi \int_0^{k_F} dk_r \int_0^{\pi} dk_\vartheta \int_0^{2\pi} dk_\varphi \times q_r^2 \sin(q_\vartheta)\,k_r^2 \sin(k_\vartheta)\Gamma_{\vec{k}\vec{q}}(t_1)\Bigg\} \tag{35}$$

with

$$\Gamma_{\vec{k}\vec{q}}(t) = V_{\vec{k}\vec{q}}(t)\,e^{\frac{i}{\hbar}\int_0^t dt_1[\varepsilon_0(t_1)+\varepsilon_{\vec{q}}(t_1)-\varepsilon_1(t_1)-\varepsilon_{\vec{k}}]}. \tag{36}$$

For a given Auger matrix element $V_{\vec{k}\vec{q}}(t)$, the multidimensional integral in Eq. (35) can be calculated efficiently using the techniques and approximations outlined in Ref. 27. The Auger matrix element, originating from the Coulomb interaction between the (active) projectile electron and an electron from the solid, is, in general, subject to the dynamical response of the target electrons. For metallic surfaces this is an important issue, as discussed, for instance, by Alvarez *et al.*[17] It leads to the screening of the Coulomb interaction and should be at least accounted for by a statically screened Coulomb potential. For the dielectric surfaces, we are primarily interest in, however, screening is suppressed by the energy gap. We calculate therefore $V_{\vec{k}\vec{q}}(t)$ from the bare Coulomb interaction. Thereby we overestimate somewhat the strength of the Auger matrix element.

We will now seek an analytic solution to the coupled rate equations (33). As a starting point, we first take a step back and consider the isolated decay channels of resonant electron capture, resonant electron emission, and Auger deexcitation. Singling out the individual reactions in Eq. (33),

we obtain

$$\frac{dn_*^{(0)}(t)}{dt} = -\Gamma_0(t)\, n_*^{(0)}(t), \tag{37a}$$

$$\frac{dn_-^{(1)}(t)}{dt} = -\Gamma_1(t)\, n_-^{(1)}(t), \tag{37b}$$

$$\frac{dn_*^{(A)}(t)}{dt} = -\Gamma_A(t)\, n_*^{(A)}(t). \tag{37c}$$

The superscripts (0), (1), and (A) identify the isolated resonant electron capture, resonant electron emission, and Auger deexcitation, respectively. Since the channels are isolated, each of the decay equations (37) comes with an analogous equation for the species that is produced. For instance, accompanying Eq. (37a) is the equation

$$\frac{dn_-^{(0)}(t)}{dt} = \Gamma_0(t)\, n_*^{(0)}(t). \tag{38}$$

The time derivatives of $n_*^{(0)}$ and $n_-^{(0)}$ differ, however, only in sign. Hence, $n_-^{(0)}$ is given through the conservation of particles as $n_-^{(0)} = 1 - n_*^{(0)}$ (valid when the channels are isolated). Consequently, the additional equations of type (38) do not contain any additional information and can be omitted. Using the initial condition $n_*^{(0)}(t_0) = n_*^{(A)}(t_0) = 1$, the system (37) can be solved straightforwardly. The result is

$$n_*^{(0)}(t) = e^{-\int_{t_0}^{t} dt_1\, \Gamma_0(t)}, \tag{39a}$$

$$n_-^{(1)}(t) = n_-^{(1)}(t')\, e^{-\int_{t'}^{t} dt_1\, \Gamma_1(t)}, \tag{39b}$$

$$n_*^{(A)}(t) = e^{-\int_{t_0}^{t} dt_1\, \Gamma_A(t)}. \tag{39c}$$

Now we are in position to use these occupancies to calculate the solution of the full, coupled system of rate equations (33). First, we consider the equation for n_*. Using the initial condition $n_*(t_0) = 1$, Eq. (33b) can be solved by separation of variables and yields

$$n_*(t) = e^{-\int_{t_0}^{t} dt_1 [\Gamma_0(t_1)+\Gamma_1(t_1)]} = n_*^{(0)}(t)\, n_*^{(A)}(t). \tag{40}$$

To solve Eq. (33a) for the occupancy of the negative ion state, we first multiply this equation by a factor $\exp[\int_{t_0}^{t} dt_2\, \Gamma_1(t_2)]$ and rearrange the terms to obtain

$$\frac{d}{dt}\left[n_-(t)\, e^{\int_{t_0}^{t} dt_2\, \Gamma_1(t_2)}\right] = \Gamma_0(t)\, n_*(t)\, e^{\int_{t_0}^{t} dt_2\, \Gamma_1(t_2)}. \tag{41}$$

Relabeling then t as t_1 and integrating the equation from $t_1 = t_0$ to $t_1 = t$, while minding the initial condition $n_-(t_0) = 0$ yields, after a further rearrangement,

$$\begin{aligned} n_-(t) &= \int_{t_0}^{t} dt_1\, \Gamma_0(t_1)\, n_*(t_1)\, e^{-\int_{t_1}^{t} dt_2\, \Gamma_1(t_2)} \\ &= \int_{t_0}^{t} dt_1 \left[-\frac{dn_*^{(0)}(t_1)}{dt_1}\right] n_*^{(A)}(t_1)\, \frac{n_-^{(1)}(t)}{n_-^{(1)}(t_1)}. \end{aligned} \tag{42}$$

Finally, the occupancy of the molecular ground state n_g, that is, the solution of Eq. (33c), is given through the particle conservation property of the full system (33),

$$n_g(t) = 1 - n_*(t) - n_-(t). \tag{43}$$

Note, the molecular occupancies satisfying the combined rate equation scheme Eqs. (40), (42), and (43) are completely determined by the occupancies $n_*^{(0)}$, $n_-^{(1)}$, and $n_*^{(A)}$. Moreover, when the Auger channel is disabled by setting $\Gamma_A(t) \equiv 0$, Eqs. (40), (42), and (43) reduce to the rate equations derived by intuitive means for the isolated RCT channel.[28] Hence the quantum kinetic treatment justifies a posteriori the intuitive approach taken by us in Ref. 28.

We now turn to the spectrum of the emitted electron. While the evolution of the $\vec{q}$ states has not been considered explicitly in our quantum kinetic calculation, the occupancy of these states can nevertheless be extracted from the solution of Eq. (33).

From the reactions (1) and (2), it is obvious that the probability for emitting an electron $n_e(t)$ is equal to the occupancy of the ground state $n_g(t)$ as every ground-state molecule must have resulted from the reaction chain and, hence, must be accompanied by an emitted electron. Consequently, the evolution of $n_e(t)$ is governed by Eq. (33c). Due to the image potential, however, not every emitted electron can escape the surface. In particular, the escape is only possible when the emitted electron's perpendicular kinetic energy $\varepsilon_{q_z}^{\infty} = \varepsilon_{\vec{q}}^{\infty} \cos^2(q_\vartheta)$ is higher than the absolute value of the image potential V_i at the position of emission. The latter can be approximated by the position of the molecule's center of mass at the time of emission.

To incorporate the image potential effect, we adopt a two step strategy. As a start, we introduce the spectral rates $\varrho_1(\varepsilon_{\vec{q}}^{\infty},t)$ and $\varrho_A(\varepsilon_{\vec{q}}^{\infty},t)$, which are not restricted by the image potential effect by writing

$$\Gamma_{1/A}(t) = \int_0^{\infty} d\varepsilon_{\vec{q}}^{\infty}\, \varrho_{1/A}\big(\varepsilon_{\vec{q}}^{\infty},t\big), \tag{44}$$

and afterwards, we let $\varrho_{1/A} \to \bar{\varrho}_{1/A}$ with

$$\begin{aligned} \bar{\varrho}_{1/A}\big(\varepsilon_{\vec{q}}^{\infty},t\big) = \int_0^{\frac{\pi}{2}} dq_\vartheta \int_0^{2\pi} dq_\varphi \Theta\big\{V_i[z_R(t)] + \varepsilon_{q_z}^{\infty}\big\} \\ \times \frac{d^2\varrho_{1/A}\big(\varepsilon_{\vec{q}}^{\infty},t\big)}{dq_\vartheta\, dq_\varphi}. \end{aligned} \tag{45}$$

An explicit expression for the spectral RCT emission rate ϱ_1 has been given in Ref. 28. The spectral Auger rate ϱ_A may be calculated from Eq. (35) by stripping out the q_r integral and multiplying the result by $m_e/\hbar^2 q_r$. Introducing the spectral decomposition of the rates in Eq. (33c) and identifying n_g with $\bar{n}_e$, we obtain

$$\frac{d\bar{n}(t)}{dt} = \int_0^{\infty} d\varepsilon_{\vec{q}}^{\infty}\, \bar{\varrho}_1\big(\varepsilon_{\vec{q}}^{\infty},t\big) n_-(t) + \int_0^{\infty} d\varepsilon_{\vec{q}}^{\infty}\, \bar{\varrho}_A\big(\varepsilon_{\vec{q}}^{\infty},t\big) n_*(t), \tag{46}$$

where $\bar{n}_e$ denotes the probability for emitting an electron that can escape from the surface. Integrating over the time argument with the initial condition $\bar{n}_e(t_0) = 0$ and taking the derivative with respect to $\varepsilon_{\vec{q}}^{\infty}$, we find for the spectrum of the emitted electron at time t,

$$\left.\frac{d\bar{n}_e}{d\varepsilon_{\vec{q}}^{\infty}}\right|_t = \int_{t_0}^{t} dt_1 \bar{\varrho}_1\big(\varepsilon_{\vec{q}}^{\infty},t_1\big) n_-(t_1) + \int_{t_0}^{t} dt_1 \bar{\varrho}_A\big(\varepsilon_{\vec{q}}^{\infty},t_1\big) n_*(t_1). \tag{47}$$

The secondary electron emission coefficient γ_e, that is, the probability for having emitted an electron after the collision is

completed, is given by

$$\gamma_e = \bar{n}_e(\infty). \tag{48}$$

The occupancies of the molecular pseudoparticle states (40), (42), and (43) and the spectrum of the emitted electron (47) are the main result of this work. The occupancies fully characterize the temporal evolution of the deexcitation of a metastable $N_2(^3\Sigma_u^+)$ molecule at a surface when both the RCT and the Auger channel are open. The ingredients required as an input, the occupancies arising from the isolated processes $n_*^{(0)}$, $n_-^{(1)}$, $n_*^{(A)}$ and the image potential adjusted spectral rates $\bar{\varrho}_1$, $\bar{\varrho}_A$, can be obtained from the quantum kinetic calculation and thus from the semiempirical model.

Assuming the parameters of the model Hamiltonian to be *a priori* fixed, either by experiment or by quantum chemical calculations, there is no free parameter in the kinetic equations that can be *a posteriori* adjusted to experimental data concerning the surface collision itself. This is in contrast to Hagstrum's theory of secondary electron emission[40,41] where the matrix elements (more precisely the combined density of states) are directly fitted to the outcome of the surface scattering experiment.

VI. NUMERICAL RESULTS

In this section, we present numerical results based on the semiclassical equations of Sec. V. We consider the particular case of a diamond surface and restrict our investigations to normal incident with a molecular kinetic energy of 50 meV. The turning point of the molecule's trajectory is then 4.4 Bohr radii.[42] As in our previous work,[27,28] we treat only the two principal orientations of the metastable $N_2(^3\Sigma_u^+)$ molecule: molecular axis perpendicular to the surface and molecule axis parallel to the surface. Furthermore, we omit the surface induced decay channel by setting $\Gamma_1(t) = \Gamma_n$. As our previous investigations showed, this is an excellent approximation.[28]

The numerics necessary to calculate within the semiempirical model the Auger matrix element $V_{\vec{k}\vec{q}}$ has been described in Ref. 27. Utilizing the fact that for the low collision energies we are interested in, the turning point of the molecule is far outside the solid as well as the fact that the LCAO wave functions are strongly localized on the molecule, whereas the wave functions of the solid and free electron are bounded in the mathematical sense, we split off the time dependence of the matrix element and integrate the rest by an interpolative grid-based Monte Carlo scheme. The tunneling matrix elements $V_{\vec{k}}$ and $V_{\vec{q}}$ can be calculated within the semiempirical model partly analytically and partly numerically. The required tools are given in Ref. 28.

First, we investigate the validity of the semiclassical approximation. As outlined above, approximations of the form (31) are only acceptable if the functions $\widetilde{\sigma}_{\vec{k}}(t_1,t_2)$ and $\widetilde{\sigma}_{\vec{k}\vec{q}}(t_1,t_2)$ are sufficiently peaked on the time diagonal $t_1 = t_2$. In order to validate this assumption for our case, we plot in Fig. 4 for the perpendicular orientation the variation of these two functions along the antidiagonal $t_1 = -t_2$. The plots can be generated directly from the definitions (22) and represent profiles with respect to the time diagonal.

For both functions $\widetilde{\sigma}_{\vec{k}}(t_1,t_2)$ and $\widetilde{\sigma}_{\vec{k}\vec{q}}(t_1,t_2)$, the real part has its maximum on the time diagonal, whereas the imaginary part vanishes on the diagonal itself but exhibits the highest value

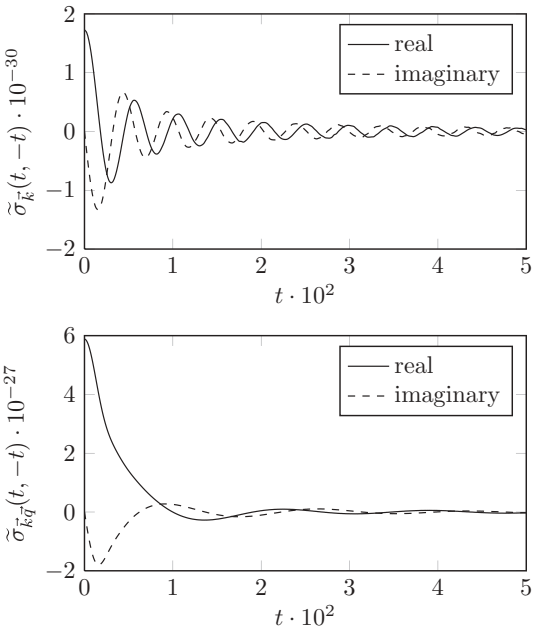

FIG. 4. Variation of the real (solid line) and imaginary (dashed line) parts of $\widetilde{\sigma}_{\vec{k}}(t_1,t_2)$ (upper panel) and $\widetilde{\sigma}_{\vec{k}\vec{q}}(t_1,t_2)$ (lower panel) as calculated from Eq. (22) along the antidiagonal $t_1 = -t_2 = t$. The molecule's axis was aligned perpendicular to the surface and the molecule's kinetic energy was fixed to 50 meV. The behavior for negative time arguments t is omitted since the real (imaginary) part of both functions is symmetric (antisymmetric) with respect to the time diagonal. Note that the time t is dimensionless. It relates to the physical time t_{phys} via $t_{\text{phys}} = a_B \Delta t / 2v_0$.

very close to it. When the time separation from the diagonal is enlarged, both functions decrease in an oscillating way. For $\widetilde{\sigma}_{\vec{k}}$, the amplitude decreases to about 10% over a dimensionless time interval of $\Delta t \approx 0.05$. This relates to a physical time span of $\Delta t_{\text{phys}} = a_B \Delta t / 2v_0 \approx 2.25$ fs and to the motion of the molecule along a distance of $0.025\, a_B$. For $\widetilde{\sigma}_{\vec{k}\vec{q}}$, the fall off is even more drastic. The behavior for shifted antidiagonals as well as for parallel orientation is very similar and hence not shown here. Altogether, we can conclude that with respect to the macroscopic motion of the molecule the functions $\widetilde{\sigma}_{\vec{k}}$ and $\widetilde{\sigma}_{\vec{k}\vec{q}}$ are indeed sufficiently peaked on the time diagonal. Thus the semiclassical approximation is valid in our case.

We now turn to the occupancies of the molecular pseudoparticle states, that is, the probabilities with which the molecular configurations involved in the deexcitation process appear in the course of the scattering event. The time-dependent occupancy of the ground state n_g, the metastable state n_*, and negative ion state n_- can be calculated from Eqs. (40), (42), and (43), respectively. The results are depicted in a semilogarithmic plot in Fig. 5.

Inspection of the curves in Fig. 5 reveals that even close to the surface the occupancy of the negative ion state is rather low. Hence the metastable projectile is almost immediately converted into a ground-state molecule and thus stays mostly neutral during the whole collision. In Fig. 5, this fact is recognizable at the crossing point of the n_* and n_g curves, which occurs at approximately half filling of both levels. The low occupancy of the negative ion state is caused by

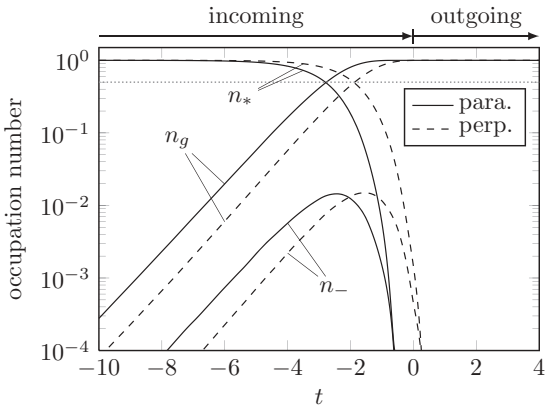

FIG. 5. Time dependence of the occupancy of the ground state molecule n_g, the metastable molecule n_*, and the negative ion n_- in the parallel (solid line) and perpendicular (dashed line) orientations. The molecule's kinetic energy was fixed to 50 meV. The dotted line represents half filling of the respective level. The y axis is logarithmic and the time is denoted in the dimensionless units of Fig. 4. The curves were calculated from Eqs. (40), (42), and (43), respectively. The incoming and outgoing branches of the trajectory are indicated at the top of the diagram.

the high efficiency of the natural decay channel[28] and not by the Auger channel destroying the metastable molecule, which is the generating species of the negative ion. In fact, it is the other way around and in order to substantiate this claim, we investigate below the relative efficiency of the RCT and Auger channels by considering the respective reaction rates. Before we do that, let us note, however, that due to the neutrality of the projectile along most of its path it would not gain much kinetic

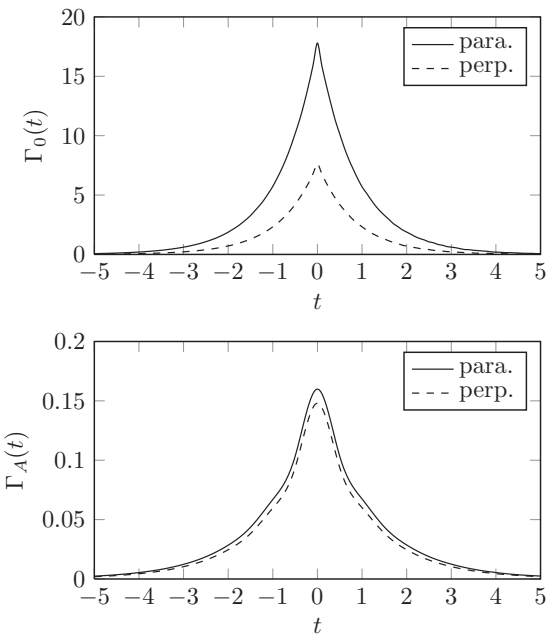

FIG. 6. Variation of the rates of resonant electron capture Γ_0 (upper panel) and Auger deexcitation Γ_A (lower panel) for the parallel (solid line) and perpendicular (dashed line) orientations at a kinetic energy of 50 meV. The time is denoted in the dimensionless units of Fig. 4.

energy in front of a charged surface. We expect therefore the semiclassical approximation and hence the rate equations to be also valid in case the deexcitation occurred in front of a negatively charged plasma wall.

Figure 6 shows the rates of resonant electron capture Γ_0 and Auger deexcitation Γ_A. For both channels, the rates are highest at the molecule's turning point (approximately $4.4a_B$), which is the point of smallest molecule-surface separation and strongest molecule-surface interaction. When the molecule-surface distance is increased, the rates decrease exponentially. The RCT channel's rate is about two orders of magnitude higher than the Auger channel's rate. Consequently, the RCT channel captures surface electrons much more efficiently than the Auger channel. In fact, the RCT channel is so effective in capturing electrons that it underruns the Auger channel by destroying its starting basis, the metastable state. As a result, in the combined two-channel system the Auger channel's performance is significantly diminished as compared to the isolated Auger reaction.

This conclusion may be verified by considering the term in the rate equations which is responsible for the production of the ground state molecule by an Auger deexcitation. It is given by [see Eqs. (33c) and (40)]

$$\Gamma_A(t)\, n_*(t) = \Gamma_A(t)\, n_*^{(A)}(t)\, n_*^{(0)}(t). \tag{49}$$

Here, the factor $n_*^{(0)}(t)$ is only present in the combined two-channel system but not in the isolated Auger system. Without explicit proof but based on numerical observations, we note that the term $n_*^{(0)}(t)$ is almost identical to the combined

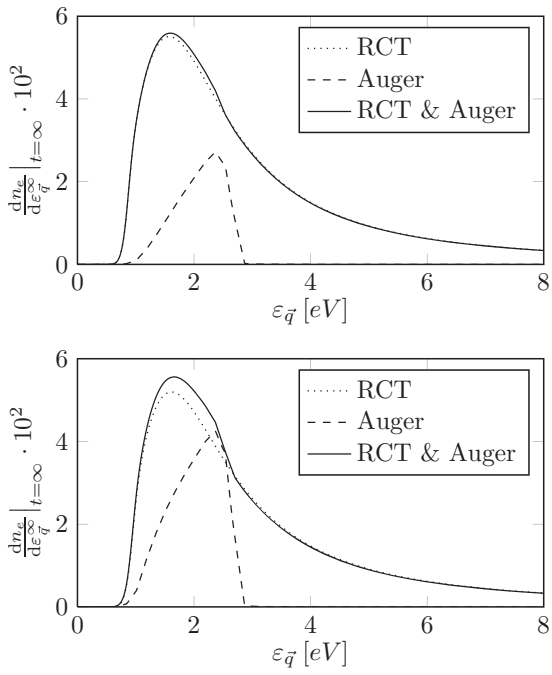

FIG. 7. Energy spectrum of the emitted electron in parallel (upper panel) and perpendicular (lower panel) orientation calculated from (47) at $t = \infty$ for a kinetic energy of 50 meV. In both panels, the dotted line specifies the isolated RCT spectrum (obtained by setting $\bar{\varrho}_A \equiv 0$), the dashed line denotes the isolated Auger spectrum (obtained by setting $\bar{\varrho}_1 \equiv 0$), and the solid line represents the combined two-channel spectrum.

TABLE I. Secondary electron emission coefficients in parallel ($\gamma_e^{\parallel}$) and perpendicular ($\gamma_e^{\perp}$) orientation at a kinetic energy of 50 meV.

	$\gamma_e^{\parallel}$	$\gamma_e^{\perp}$
RCT	0.16685	0.15873
Auger	0.02760	0.04921
RCT and Auger	0.16754	0.16335

occupation $n_*(t)$ depicted in Fig. 5. Hence, in the combined system, the Auger channel's ground-state production term (49) is strongly suppressed already in the incoming branch of the trajectory.

Finally, we turn to the energy spectrum of the emitted electron. Figure 7 depicts the emission spectrum at $t = \infty$ for the combined two-channel reaction as well as for the isolated reaction channels. The latter can be obtained by setting in (47) $\bar{\varrho}_A \equiv 0$ or $\bar{\varrho}_1 \equiv 0$. As can be seen, the isolated RCT spectra exhibit a strong peak at about 1.5 eV and slowly drop off for higher energies. The isolated Auger spectra, on the other hand, monotonously increase until approximately 2.8 eV and then immediately fall off. The low energy cutoff of all curves is due to the trapping of the emitted electron in the image potential close to the surface when its perpendicular energy is too low. The combined spectra almost equal the respective isolated RCT spectra. Only in the range from 1.5 to 2.5 eV, the combined spectra are slightly increased with respect to the RCT curves. This minor enlargement is due to the Auger channel and supports our previous finding that the RCT channel dominates the Auger channel.

The combined spectra in Fig. 7 are different from the simple addition of the isolated spectra. This behavior is caused by the unified treatment of the RCT and Auger reaction channels. The effect would be even more pronounced for molecular species forming stable negative ions. Here the resonant electron emission would be almost completely blocked as the surface induced decay is always very weak. The resonant electron capture, however, would be still very efficient in destroying the initial species. Consequently, the spectrum of the emitted electron would resemble the Auger spectrum in shape but would be strongly decreased in magnitude.

The secondary electron emission coefficients are given by the area beneath the curves in Fig. 7 and are summarized in Table I. In accordance with our previous observations, the emission coefficients are not changed significantly by the inclusion of the Auger channel. A similar result was found by Stracke *et al.*[25] for $N_2(^3\Sigma_u^+)$ deexciting at a tungsten surface. Their experimental measurements imply that only about 10% of the secondary electron emission coefficient is made up by the Auger channel.

VII. CONCLUSIONS

We constructed in this work a semiempirical generalized Anderson-Newns model for secondary electron emission due to deexcitation of metastable $N_2(^3\Sigma_u^+)$ molecules at dielectric surfaces. The model treats Auger deexcitation and the two-step resonant charge transfer process, where the $N_2^-(^2\Pi_g)$ ion acts as a relay state, on an equal footing. It reduces the molecular projectile to a two-level system representing the molecular orbitals which change their occupancies during the reaction and treats the surface as a simple step potential confining the electrons of the solid. By construction, the semiempirical model is not restricted to a particular projectile-target combination. Having applications of the model to charge-transferring processes at plasma walls in mind, where a great variety of different projectile-target combinations occurs, we consider this as a real advantage. Another advantage is that the semiempirical model separates the many-body theoretical description of the noninteracting projectile and target from the quantum kinetic treatment of the scattering process. The former is simply encapsulated in the parameters of the model Hamiltonian and the latter is performed by Green functions. This is particularly advantageous in cases where the surface scattering event is studied primarily because of its connection to the physics of quantum impurities.

For the semiempirical model to work, a method was required to assign and control the energies of the two-level system in accordance to the reaction channels, that is, to have the two-level system describing all three molecular configurations involved in the deexcitation process: the metastable $N_2(^3\Sigma_u^+)$ molecule, the negative ion $N_2^-(^2\Pi_g)$, and the molecular ground state $N_2(^1\Sigma_g^+)$. We showed how this can be done with projection operators and auxiliary bosons. As a result, both the resonant tunneling and the Auger channel could be cast into a single model Hamiltonian which, with the help of pseudoparticle operators, could then be made amenable to a diagrammatic quantum kinetic calculation. Using the self-consistent noncrossing approximation for the self-energies and a saddle-point approximation for the time integrals in the self-energies, we finally derived from the Dyson equations for the propagators of the molecular pseudoparticles a set of rate equations for the probabilities with which the molecular configurations contributing to the deexcitation process can be found in the course of the scattering event. Without the Auger channel, the system of rate equations reduces to the one postulated by us before on intuitive grounds for the RCT channel alone.[28] The present work justifies therefore this reasoning *a posteriori*.

For the particular case of a diamond surface, we verified the validity of the semiclassical approximation and investigated for a collision energy of 50 meV the interplay of the resonant tunneling and the Auger channel. In particular, we analyzed the temporal evolution of the probabilities with which the projectile is to be found in the $N_2(^3\Sigma_u^+)$, the $N_2^-(^2\Pi_g)$, or the $N_2(^1\Sigma_g^+)$ state and explicitly calculated the rates for electron capture due, respectively, to tunneling and Auger deexcitation. We also obtained the spectrum of the emitted electron and the secondary electron emission coefficient γ, which are the two quantities of main importance for the modeling of gas discharges. Our results indicate for a diamond surface and a kinetic energy of 50 meV, the resonant tunneling channel clearly dominating the Auger channel. The contribution of the Auger channel to the secondary electron emission coefficient lies only in the range of a few percent. The overall γ coefficient is on the order of 10^{-1} in agreement with what has to be typically assumed to make kinetic simulations of dielectric barrier discharges reproduce the properties of the discharge.

With minor modifications the semiempirical model and its quantum kinetic handling leading to the easy to use set of

rate equations can be adopted to other plasma-relevant charge-transferring surface collisions as well. At least for low-energy collisions, where the projectile velocities are low enough to allow for a reduction of the full double-time kinetic equations to a set of simple rate equations, we can thus hope to replace the rules of the thumb that are often needed to characterize secondary electron emission due to neutral and charged heavy plasma species hitting the plasma wall by plausible quantitative estimates.

ACKNOWLEDGMENTS

Johannes Marbach was funded by the federal state of Mecklenburg-Western Pomerania through a postgraduate scholarship. In addition, this work was supported by the Deutsche Forschungsgemeinschaft through the Transregional Collaborative Research Center SFB/TRR24.

APPENDIX A: LANGRETH-WILKINS RULES

The Langreth-Wilkins rules[35] are a powerful tool for the analytic continuation of propagators defined on a complex time contour onto the real time axis. Their explicit form depends on the initial definition of the Green functions. Unfortunately, there is no common agreement about the usage of i factors. Moreover, rules published in the past sometimes contained typographic errors.[31] Due to these reasons, we list the explicit form of the Langreth-Wilkins rules used in this work. The rules can be derived in the standard way[35,43] using, however, the definitions (17)–(19) for the Green functions. In the following, F and B denote fermion and boson propagators, respectively.

To analytically continue the bosonlike fermion-antifermion pair,

$$B(t,t') = F_1(t,t')\,F_2(t',t), \tag{A1}$$

we utilize

$$B^{>}(t,t') = i\,F_1^{>}(t,t')\,F_2^{<}(t',t), \tag{A2a}$$
$$B^{<}(t,t') = i\,F_1^{<}(t,t')\,F_2^{>}(t',t), \tag{A2b}$$
$$B^{R}(t,t') = i\big[F_1^{<}(t,t')\,F_2^{A}(t',t) + F_1^{R}(t,t')\,F_2^{<}(t',t)\big], \tag{A2c}$$
$$B^{A}(t,t') = i\big[F_1^{<}(t,t')\,F_2^{R}(t',t) + F_1^{A}(t,t')\,F_2^{<}(t',t)\big]. \tag{A2d}$$

For the fermion-like fermion-boson pair

$$F(t,t') = F_1(t,t')\,B_1(t,t'), \tag{A3}$$

the following rules hold:

$$F^{>}(t,t') = -i\,F_1^{>}(t,t')\,B_1^{>}(t,t'), \tag{A4a}$$
$$F^{<}(t,t') = -i\,F_1^{<}(t,t')\,B_1^{<}(t,t'), \tag{A4b}$$
$$F^{R}(t,t') = -i\big[F_1^{R}(t,t')\,B_1^{<}(t,t') + F_1^{>}(t,t')\,B_1^{R}(t,t')\big], \tag{A4c}$$
$$F^{A}(t,t') = -i\big[F_1^{A}(t,t')\,B_1^{<}(t,t') + F_1^{>}(t,t')\,B_1^{A}(t,t')\big]. \tag{A4d}$$

The bosonlike boson-boson pair

$$B(t,t') = B_1(t,t')\,B_2(t,t'), \tag{A5}$$

can be analytically continued by

$$B^{>}(t,t') = -i\,B_1^{>}(t,t')\,B_2^{>}(t,t'), \tag{A6a}$$
$$B^{<}(t,t') = -i\,B_1^{<}(t,t')\,B_2^{<}(t,t'), \tag{A6b}$$
$$B^{R}(t,t') = -i\big[B_1^{R}(t,t')\,B_2^{>}(t,t') + B_1^{<}(t,t')\,B_2^{R}(t,t')\big], \tag{A6c}$$
$$B^{A}(t,t') = -i\big[B_1^{A}(t,t')\,B_2^{>}(t,t') + B_1^{<}(t,t')\,B_2^{A}(t,t')\big]. \tag{A6d}$$

Finally, to analytically continue the bosonlike boson-antiboson pair

$$B(t,t') = B_1(t,t')\,B_2(t',t), \tag{A7}$$

we use

$$B^{>}(t,t') = -i\,B_1^{>}(t,t')\,B_2^{<}(t',t), \tag{A8a}$$
$$B^{<}(t,t') = -i\,B_1^{<}(t,t')\,B_2^{>}(t',t), \tag{A8b}$$
$$B^{R}(t,t') = -i\big[B_1^{<}(t,t')\,B_2^{A}(t',t) + B_1^{R}(t,t')\,B_2^{<}(t',t)\big], \tag{A8c}$$
$$B^{A}(t,t') = -i\big[B_1^{<}(t,t')\,B_2^{R}(t',t) + B_1^{A}(t,t')\,B_2^{<}(t',t)\big]. \tag{A8d}$$

Furthermore, for the analytic continuation of the contour integrals within the Dyson equations, we also need to project terms of the form

$$D(t,t') = \int_{\mathcal{C}} dt_1\,D_1(t,t_1)\,D_2(t_1,t'), \tag{A9}$$

where D, D_1, and D_2 are either fermion-like or bosonlike. This can be accomplished by the rules

$$D^{<}(t,t') = \int_{-\infty}^{\infty} dt_1\big[D_1^{R}(t,t_1)D_2^{<}(t_1,t') + D_1^{<}(t,t_1)D_2^{A}(t_1,t')\big], \tag{A10a}$$
$$D^{>}(t,t') = \int_{-\infty}^{\infty} dt_1\big[D_1^{R}(t,t_1)D_2^{>}(t_1,t') + D_1^{>}(t,t_1)D_2^{A}(t_1,t')\big], \tag{A10b}$$
$$D^{R}(t,t') = \int_{-\infty}^{\infty} dt_1\;D_1^{R}(t,t_1)\,D_2^{R}(t_1,t'), \tag{A10c}$$
$$D^{A}(t,t') = \int_{-\infty}^{\infty} dt_1\;D_1^{A}(t,t_1)\,D_2^{A}(t_1,t'). \tag{A10d}$$

APPENDIX B: DYSON EQUATIONS

In this appendix, we summarize the Dyson equations for the analytic pieces of the molecular Green functions G_{-}, B_{*}, and B_g as obtained by an application of the Langreth-Wilkins rules of appendix A to the self-energies shown in Fig. 3.

The lesser Green functions satisfy

$$\left[i\frac{\partial}{\partial t}-\frac{\varepsilon_-(t)}{\hbar}\right]G^<_-(t,t') = \int_{-\infty}^{t} dt_1\big[\sigma^>_{\vec{k}}(t,t_1)\,B^R_*(t,t_1)\,G^<_-(t_1,t') + \sigma^R_{\vec{k}}(t,t_1)\,B^<_*(t,t_1)\,G^<_-(t_1,t') + \sigma^>_{\vec{q}}(t,t_1)\,B^R_g(t,t_1)\,G^<_-(t_1,t') + \sigma^R_{\vec{q}}(t,t_1)\,B^<_g(t,t_1)\,G^<_-(t_1,t')\big] + \int_{-\infty}^{t'} dt_1[\sigma^<_{\vec{k}}(t,t_1)\,B^<_*(t,t_1)\,G^A_-(t_1,t') + \sigma^<_{\vec{q}}(t,t_1)\,B^<_g(t,t_1)\,G^A_-(t_1,t')], \tag{B1a}$$

$$\left[i\frac{\partial}{\partial t}-\frac{\varepsilon_*(t)}{\hbar}\right]B^<_*(t,t') = \int_{-\infty}^{t} dt_1\big[\sigma^<_{\vec{k}}(t_1,t)\,G^R_-(t,t_1)\,B^<_*(t_1,t') + \sigma^A_{\vec{k}}(t_1,t)\,G^<_-(t,t_1)\,B^<_*(t_1,t') + i\sigma^>_{\vec{k}\vec{q}}(t,t_1)\,B^R_g(t,t_1)\,B^<_*(t_1,t') + i\sigma^R_{\vec{k}\vec{q}}(t,t_1)\,B^<_g(t,t_1)\,B^<_*(t_1,t')\big] + \int_{-\infty}^{t'} dt_1[\sigma^>_{\vec{k}}(t_1,t)\,G^<_-(t,t_1)\,B^A_*(t_1,t') + i\sigma^<_{\vec{k}\vec{q}}(t,t_1)\,B^<_g(t,t_1)\,B^A_*(t_1,t')], \tag{B1b}$$

$$\left[i\frac{\partial}{\partial t}-\frac{\varepsilon_g(t)}{\hbar}\right]B^<_g(t,t') = \int_{-\infty}^{t} dt_1\big[\sigma^<_{\vec{q}}(t_1,t)\,G^R_-(t,t_1)\,B^<_g(t_1,t') + \sigma^A_{\vec{q}}(t_1,t)\,G^<_-(t,t_1)\,B^<_g(t_1,t') + i\sigma^<_{\vec{k}\vec{q}}(t_1,t)\,B^R_*(t,t_1)\,B^<_g(t_1,t') + i\sigma^A_{\vec{k}\vec{q}}(t_1,t)\,B^<_*(t,t_1)\,B^<_g(t_1,t')\big] + \int_{-\infty}^{t'} dt_1\big[\sigma^>_{\vec{q}}(t_1,t)\,G^<_-(t,t_1)\,B^A_g(t_1,t') + i\sigma^>_{\vec{k}\vec{q}}(t_1,t)\,B^<_*(t,t_1)\,B^A_g(t_1,t')\big], \tag{B1c}$$

while the retarded Green functions obey

$$\left[i\frac{\partial}{\partial t}-\frac{\varepsilon_-(t)}{\hbar}\right]G^R_-(t,t') = \delta(t-t') + \int_{t'}^{t} dt_1\big[\sigma^>_{\vec{k}}(t,t_1)\,B^R_*(t,t_1)\,G^R_-(t_1,t') + \sigma^R_{\vec{k}}(t,t_1)\,B^<_*(t,t_1)\,G^R_-(t_1,t') + \sigma^>_{\vec{q}}(t,t_1)\,B^R_g(t,t_1)\,G^R_-(t_1,t') + \sigma^R_{\vec{q}}(t,t_1)\,B^<_g(t,t_1)\,G^R_-(t_1,t')\big], \tag{B1d}$$

$$\left[i\frac{\partial}{\partial t}-\frac{\varepsilon_*(t)}{\hbar}\right]B^R_*(t,t') = \delta(t-t') + \int_{t'}^{t} dt_1\big[\sigma^<_{\vec{k}}(t_1,t)\,G^R_-(t,t_1)\,B^R_*(t_1,t') + \sigma^A_{\vec{k}}(t_1,t)\,G^<_-(t,t_1)\,B^R_*(t_1,t') + i\sigma^>_{\vec{k}\vec{q}}(t,t_1)\,B^R_g(t,t_1)\,B^R_*(t_1,t') + i\sigma^R_{\vec{k}\vec{q}}(t,t_1)\,B^<_g(t,t_1)\,B^R_*(t_1,t')\big], \tag{B1e}$$

$$\left[i\frac{\partial}{\partial t}-\frac{\varepsilon_g(t)}{\hbar}\right]B^R_g(t,t') = \delta(t-t') + \int_{t'}^{t} dt_1\big[\sigma^<_{\vec{q}}(t_1,t)\,G^R_-(t,t_1)\,B^R_g(t_1,t') + \sigma^A_{\vec{q}}(t_1,t)\,G^<_-(t,t_1)\,B^R_g(t_1,t') + i\sigma^<_{\vec{k}\vec{q}}(t_1,t)\,B^R_*(t,t_1)\,B^R_g(t_1,t') + i\sigma^A_{\vec{k}\vec{q}}(t_1,t)\,B^<_*(t,t_1)\,B^R_g(t_1,t')\big]. \tag{B1f}$$

The greater and advanced Green function can be obtained from the definitions (19) and the symmetry relations (20).

*marbach@physik.uni-greifswald.de

[1] *Slow Heavy-Particle Induced Electron Emission from Solid Surface*, edited by H.-P. Winter and J. Burgdörfer (Springer-Verlag, Berlin Heidelberg, 2007).

[2] *Low Energy Ion-Surface Interaction*, edited by J. W. Rabalais (Wiley, New York, 1994).

[3] X. He and J. A. Yarmoff, Phys. Rev. Lett. **105**, 176806 (2010).

[4] J. Merino and J. B. Marston, Phys. Rev. B **58**, 6982 (1998).

[5] H. Shao, D. C. Langreth, and P. Nordlander, Phys. Rev. B **49**, 13929 (1994).

[6] *The Kondo Problem to Heavy Fermions*, edited by A. C. Hewson (Cambridge University Press, Cambridge, 1993).

[7] *Single Charge Tunneling: Coulomb Blockade Phenomena in Nanostructures*, edited by H. Grabert and M. H. Devoret (Plenum Press, New York, 1992).

[8] M. A. Lieberman and A. J. Lichtenberg, *Principles of Plasma Discharges and Materials Processing* (Wiley-Interscience, New York, 2005).

[9] R. Brandenburg, V. A. Maiorov, Y. B. Golubovskii, H.-E. Wagner, J. Behnke, and J. F. Behnke, J. Phys. D **38**, 2187 (2005).

[10] F. Massines, S. P., N. Gherardi, C. Khamphan, and A. Ricard, Surf. Coat. Technol. **174–175**, 8 (2003).

[11] K. H. Becker, K. H. Schoenbach, and J. G. Eden, J. Phys. D **39**, R55 (2006).

[12] K. J. Snowdon, R. Hentschke, A. Närmann, W. Heiland, E. Mühling, and W. Eckstein, Nucl. Instrum. Methods Phys. Res., Sect. B **23**, 309 (1987).

[13] R. Zimny, Z. L. Miskovic, N. N. Nedeljkovic, and L. D. Nedeljkovic, Surf. Sci. **255**, 135 (1991).

[14] A. V. Onufriev and J. B. Marston, Phys. Rev. B **53**, 13340 (1996).

[15] C. A. Keller, A. C. Lavery, and B. H. Cooper, Phys. Rev. B **58**, 10959 (1998).

[16] N. Lorente, M. A. Cazalilla, J. P. Gauyacq, D. Teillet-Billy, and P. M. Echenique, Surf. Sci. **411**, L888 (1998).

[17] M. A. Vicente Alvarez, V. H. Ponce, and E. C. Goldberg, Phys. Rev. B **57**, 14919 (1998).

[18]E. C. Goldberg, R. Monreal, F. Flores, H. H. Brongersma, and P. Bauer, Surf. Sci. **440**, L875 (1999).
[19]R. T. Pepino and G. G. Kleiman, Solid State Commun. **124**, 317 (2002).
[20]N. P. Wang, E. A. García, R. Monreal, F. Flores, E. C. Goldberg, H. H. Brongersma, and P. Bauer, Phys. Rev. A **64**, 012901 (2001).
[21]E. A. García, N. P. Wang, R. C. Monreal, and E. C. Goldberg, Phys. Rev. B **67**, 205426 (2003).
[22]W. Heiland, in *Low Energy Ion-Surface Interaction*, edited by J. W. Rabalais (Wiley, New York, 1994), p. 313.
[23]U. Imke, K. J. Snowdon, and W. Heiland, Phys. Rev. B **34**, 48 (1986).
[24]U. Imke, K. J. Snowdon, and W. Heiland, Phys. Rev. B **34**, 41 (1986).
[25]P. Stracke, F. Wiegershaus, S. Krischok, and V. Kempter, Surf. Sci. **396**, 212 (1998).
[26]N. Lorente, D. Teillet-Billy, and J. P. Gauyacq, Surf. Sci. **432**, 155 (1999).
[27]J. Marbach, F. X. Bronold, and H. Fehske, Phys. Rev. B **84**, 085443 (2011).
[28]J. Marbach, F. X. Bronold, and H. Fehske, Eur. Phys. J. D **66**, 106 (2012).
[29]P. Coleman, Phys. Rev. B **29**, 3035 (1984).
[30]N. S. Wingreen and Y. Meir, Phys. Rev. B **49**, 11040 (1994).
[31]D. C. Langreth and P. Nordlander, Phys. Rev. B **43**, 2541 (1991).
[32]R. Aguado and D. C. Langreth, Phys. Rev. B **67**, 245307 (2003).
[33]C. M. Dutta and P. Nordlander, Prog. Surf. Sci. **67**, 155 (2001).
[34]J. B. Marston, D. R. Andersson, E. R. Behringer, B. H. Cooper, C. A. DiRubio, G. A. Kimmel, and C. Richardson, Phys. Rev. B **48**, 7809 (1993).
[35]D. C. Langreth and J. W. Wilkins, Phys. Rev. B **6**, 3189 (1972).
[36]U. Kaldor, J. Chem. Phys. **81**, 2406 (1984).
[37]M. Honigmann, R. J. Buenker, and H. P. Liebermann, J. Chem. Phys. **125**, 234304 (2006).
[38]P. Kürpick and U. Thumm, Phys. Rev. A **54**, 1487 (1996).
[39]G. Carmona and J. L. Cardoso, Rev. Mex. Fis. Suppl. **48**, 010000 (2002).
[40]H. D. Hagstrum, Phys. Rev. **96**, 325 (1954).
[41]H. D. Hagstrum, Phys. Rev. **122**, 83 (1961).
[42]G. Katz and R. Kosloff, J. Chem. Phys. **103**, 9475 (1995).
[43]H. Haug and A.-P. Jauho, *Quantum Kinetics in Transport and Optics of Semiconductors* (Springer-Verlag, Berlin, 1996).